# Structure of fluoride-containing bioactive glasses

**Delia S. Brauer,*[a] Natalia Karpukhina,[a] Robert V. Law[b] and Robert G. Hill[ac]**

***Received 16th January 2009, Accepted 11th May 2009***
***First published as an Advance Article on the web 22nd June 2009***
**DOI: 10.1039/b900956f**

Fluoride prevents dental cavities, stimulates bone mineralisation and decreases the melting temperature of glasses and is therefore an interesting component of bioactive glasses for use as dental or orthopaedic biomaterials. However, when designing new glass compositions, the structural role of fluoride in the glass needs to be better understood. We have characterised a glass series in the system $SiO_2$–$P_2O_5$–CaO–$Na_2O$ with increasing concentrations of $CaF_2$. Network connectivity was fixed at 2.13 by adding $CaF_2$ while the ratio of all other components was kept constant. $^{19}F$ and $^{29}Si$ MAS NMR spectra showed that addition of $CaF_2$ does not cause disruption of the glass network by formation of Si–F bonds but forms mixed calcium sodium fluoride species. $^{31}P$ MAS NMR showed phosphate being present as orthophosphate. Hence it does not form part of the actual glass network backbone and no Si–O–P bonds are present. $^{23}Na$ MAS NMR showed the presence of multiple sodium sites with an increase in the mean coordination number of sodium with increasing $CaF_2$ content. The glass transition temperature decreased with increasing amounts of $CaF_2$. As no Si–F bonds were formed, this can be explained by formation of hypothetical $CaF^+$ species. The results can be used for designing new fluoride-containing bioactive glass compositions for specific applications.

## Introduction

Fluoride is well known to prevent dental decay by inhibiting enamel and dentine demineralisation, enhancement of remineralisation and inhibition of bacterial enzymes.[1,2] One key step in caries prevention is the formation of fluorapatite, which is more acid resistant than carbonated hydroxyapatite, the main component of enamel and dentine. Fluoride is also known to increase bone density and despite some dispute on dose and effectiveness in prevention of fractures, it is of interest for treatment of osteoporosis.[3,4] For these reasons addition of fluoride to bioactive glasses and ceramics is of great interest for the development of dental or orthopaedic biomaterials.[5,6] However, if we want to successfully design new bioactive glass compositions, we need to know the glass structure.

Bioactive glasses are known to form an intimate bond to bone due to formation of a hydroxycarbonate apatite (HCA) layer on their surface when in contact with body fluids due to dissolution processes.[7] Their bone bonding ability makes bioactive glasses of interest for use as bone replacement materials and coatings of metallic implants but also as dentifrices,[8] and in all these applications fluoride would be beneficial. The structure of silicate glasses can be described as a crosslinked inorganic polymer of oxygen and silicon. Glass properties may be explained on the basis of network connectivity (NC) which is the number of bridging oxygen atoms (BO) per network forming element.[9] Thus pure silica glass has an NC of 4 while a glass structure consisting of linear $[SiO_3]_n^{2n-}$ chains has an NC of 2. NC can be used to predict glass surface reactivity, solubility or the likelihood of undergoing glass-in-glass phase separation and bioactivity.[9,10] In general, reactivity and solubility change dramatically at a network connectivity of 2, which is the point where the glass structure changes from a crosslinked network to linear chains of decreasing molar mass. The lower the network connectivity of a glass, the lower its glass transition temperature and the greater its reactivity and solubility. Thus NC is a helpful tool when designing new bioactive glass compositions.

Solid-state nuclear magnetic resonance (NMR) is an ideal modern tool for investigation of glass structure as NMR is element specific and highly sensitive to the local chemical environment of atoms containing magnetically active nuclei. For instance, $^{19}F$ magic angle spinning (MAS) NMR is known to be an excellent technique for providing information on the local structure in fluoride-containing silicate glasses. $^{29}Si$ and $^{31}P$ MAS NMR are widely used to monitor next neighbours and the silicon and phosphorus environments in glasses and can determine the $Q^n$ structure. In addition, we take advantage of the $^{23}Na$ MAS NMR which is recognised as a sensitive probe of sodium environment in amorphous and crystalline materials.

The purpose of this study was to examine fluoride-containing bioactive glasses and the effects of fluoride incorporation on glass structure, thermal properties and temperature behaviour. We hypothesise that in these compositions, with their large number of non-bridging oxygens (NBO), fluoride does not disrupt the glass network by formation of non-bridging fluorines (NBF), but instead remains complexed to calcium. Hence $CaF_2$ was added by keeping the NC and the ratio of all other components constant. Glasses were characterised using X-ray powder diffraction, differential scanning calorimetry, $^{19}F$, $^{29}Si$, $^{31}P$ and $^{23}Na$ MAS NMR spectroscopy.

[a]*Imperial College, Department of Materials, Exhibition Road, London, UK SW7 2AZ. E-mail: d.brauer@imperial.ac.uk; Fax: +44 207 594 6757; Tel: +44 207 594 6385*
[b]*Imperial College, Department of Chemistry, Exhibition Road, London, UK SW7 2AZ*
[c]*Barts and The London, Unit of Dental and Physical Sciences, Mile End Road, London, UK E1 4NS*

**Table 1** Synthetic glass composition in mol% and theoretical network connectivity ($NC_1$ calculated assuming fluorine complexes calcium, $NC_2$ calculated assuming fluorine forms non-bridging fluorines attached to silicon)

| Glass | $SiO_2$ | $P_2O_5$ | CaO | $Na_2O$ | $CaF_2$ | $NC_1$ | $NC_2$ |
|---|---|---|---|---|---|---|---|
| A | 49.47 | 1.07 | 23.08 | 26.38 | — | 2.13 | 2.13 |
| B | 47.12 | 1.02 | 21.98 | 25.13 | 4.75 | 2.13 | 1.82 |
| C | 44.88 | 0.97 | 20.94 | 23.93 | 9.28 | 2.13 | 1.49 |
| D | 42.73 | 0.92 | 19.94 | 22.79 | 13.62 | 2.13 | 1.15 |
| E | 40.68 | 0.88 | 18.98 | 21.69 | 17.76 | 2.13 | 0.78 |
| F | 36.83 | 0.80 | 17.18 | 19.64 | 25.54 | 2.13 | −0.01 |
| G | 33.29 | 0.72 | 15.53 | 17.75 | 32.71 | 2.13 | −0.90 |
| H | 44.88 | 0.97 | 44.87 | — | 9.28 | 2.13 | 1.49 |

## Experimental

### Glass synthesis

Glasses in the system $SiO_2$–$P_2O_5$–CaO–$Na_2O$–$CaF_2$ were produced using a melt–quench route. $CaF_2$ was added in increasing amounts while the network connectivity (NC) and the ratio of all other components were kept constant (Table 1). In addition, one sodium-free glass was synthesised. Mixtures of analytical grade $SiO_2$ (Prince Minerals Ltd., UK), $P_2O_5$, $CaCO_3$, $Na_2CO_3$ and $CaF_2$ (all Sigma-Aldrich) with addition of <0.1 wt% $CoCO_3$ (Alfa Aesar) to reduce the spin–lattice relaxation times for $^{29}$Si NMR were melted in a platinum–rhodium crucible for 1 h at 1430 °C in an electric furnace (Lenton EHF 17/3). A batch size of approximately 100 g was used. After melting, the glasses were rapidly quenched into water to prevent crystallisation.

### Glass characterisation

All compositions were obtained in an amorphous state as confirmed by powder X-ray diffraction experiments (XRD; Phillips PW1700, 40 kV/40 mA, CuK$\alpha$, data collected at room temperature; results not shown). The glass transition temperature ($T_g$) and crystallisation temperatures of the glasses were determined using differential scanning calorimetry (DSC). 50 mg of glass frit were analysed in a platinum crucible using analytical grade alumina powder as reference with a heating rate of 10 K min$^{-1}$.

For investigation of crystal phases, milled glass powder was heat-treated in an analogous fashion to the DSC experiments: samples were heated to crystallisation onset ($T_{c,ons}$) temperature at a heating rate of 10 K min$^{-1}$ and then were allowed to cool to room temperature without holding at $T_{c,ons}$. Crystallised phases were analysed using XRD and NMR (see below).

### Solid-state MAS NMR

For solid-state MAS NMR experiments, the glass was ground using a Glen Creston Gy-Ro mill for 7 min. Glass structure was analysed using $^{19}$F, $^{29}$Si, $^{31}$P and $^{23}$Na MAS NMR. Experiments were performed using Bruker 200 MHz (4.7 T) and 600 MHz (14.1 T) spectrometers. $^{19}$F NMR data were collected at a Larmor frequency of 188.2 MHz under spinning conditions of 12.5 kHz in a 4 mm rotor. To avoid ringing effects from the probe, the Hahn-echo pulse sequence $\pi/2 - \tau - \pi$ was applied with a $\pi/2$ pulse of 2.35 μs and the echo delay $\tau$ of 76.5 μs. A recycle delay of 10 s was used, with 16 dummy scans performed before counting. A $^{19}$F NMR background signal thoroughly acquired on the fluorine-free glass of this series was subtracted from the spectra of the fluorine-containing glasses. The background suppression method (DEPTH) was used for $^{19}$F NMR on crystallised glasses.[11] $^{19}$F chemical shift scale was referenced using the −120 ppm peak of 1 M NaF aqueous solution as a secondary reference against $CFCl_3$. $^{29}$Si MAS NMR experiments were carried out at a Larmor frequency of 39.7 MHz and spinning speed of 4.5 kHz in a 4 mm rotor using the Hahn-echo pulse sequence with the $\pi/2$ pulse of 5.25 μs and 76.5 μs echo delay $\tau$. $^{29}$Si NMR was set up using a 3 min recycle delay. The −1.5 ppm peak of tetrakis(trimethylsilyl)methane was used for reference in $^{29}$Si NMR. $^{19}$F and $^{29}$Si NMR data were processed with 200 Hz line broadening. $^{29}$Si NMR experiments on crystallised samples were performed using 36.5 μs echo delay, and a 50 Hz exponential filter was applied to these data. $^{31}$P MAS NMR spectra were acquired at 81.0 MHz in the 4 mm rotor spinning at 4.5 kHz. 64 transients of a single pulse experiment with 2.5 μs $\pi/2$ pulse and 49 s recycle delay were collected for each sample. $^{31}$P chemical shift was referenced to the signal of 85% $H_3PO_4$. $^{23}$Na NMR was performed at 158.7 MHz in 2.5 mm and 4 mm rotors and spinning speeds of about 20–25 kHz and 15 kHz, respectively. Short pulses corresponding to the magnetisation tip angle of $\pi/12$ and 0.5 s recycle delay were used for these measurements. The spectra were referenced to a 0 ppm frequency of the signal from 1 M aqueous solution of NaCl. 50 Hz line broadening was applied before Fourier transforming of the $^{31}$P and $^{23}$Na NMR spectra. $^{23}$Na 3QMAS NMR data were obtained using a 4-pulse sequence with 20 μs zero filter. The spectra were processed with xfshear utility of Xwinnmr Bruker software and presented in a universal scale.[12]

## Results and discussion

### Structural behaviour of the silicate phase

The introduction of fluoride into a bioactive glass composition did not cause formation of detectable amounts of Si–F bonds: $^{29}$Si MAS NMR results (Fig. 1) show a peak at about −80 ppm which corresponds to $Q^2$ Si units and a shoulder at about −92

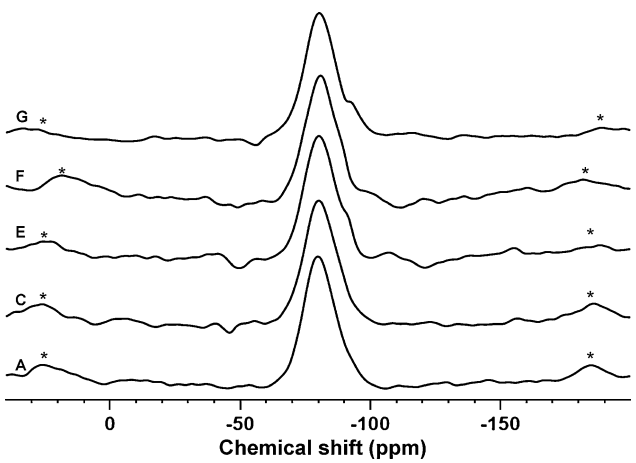


**Fig. 1** $^{29}$Si MAS NMR spectra of glasses A, C and E to G (from bottom to top). Spinning side bands are marked by an asterisk.

ppm indicating the presence of a small number of $Q^3$ Si units, which were estimated using dmfit[13] as a 10–14% contribution to the signal. This is in good agreement with NC calculations assuming fluorine is binding calcium and thus reducing the availability of calcium for forming NBO ($NC_1$, Table 1). These calculations gave an NC of 2.13 for all glasses which correspond to mainly $Q^2$ with small amounts of $Q^3$. If the network connectivity is calculated assuming fluorine forms NBF attached to Si ($NC_2$, Table 1), the values are too low to be credible. There is no change in peak position (Fig. 1) with increasing amounts of $CaF_2$, which suggests that formation of Si–F bonds does not occur (peaks would be expected to move to less negative chemical shift (towards 0 ppm) if there was formation of Si–F bonds in the glass which does not occur), but also that no significant amounts of fluorine were lost during melting. The absence of Si–F is in agreement with the findings by Lusvardi *et al.* who investigated the structure of fluoride-containing bioactive glasses by computational investigation.[14] Due to differences in glass design (Lusvardi *et al.* substituted $CaF_2$ for CaO and $Na_2O$) they found increased NC with increasing $CaF_2$ content but did not find any Si–F bonds for $CaF_2$ concentrations below 20 mol%, and even above 20 mol% the amount was negligible. This agrees with our NMR results presented here and with other previously reported experimental findings.[15–18]

After heat-treatment, the fluorine-free sample (A) shows combeite ($Na_2Ca_2Si_3O_9$) as the main crystal phase as determined by XRD (Fig. 2). It also shows some additional peaks of low intensity which we were not able to assign. With increasing amounts of $CaF_2$ in the composition, calcium fluoride ($CaF_2$, samples B to F) and cuspidine ($Ca_4Si_2O_7F_2$, samples C to F) appear as additional crystal phases. Sample G, which has the highest fluorine content gives only a single crystal phase which is calcium fluoride. Sodium-free sample H only crystallised to a small degree and therefore the XRD pattern shows only a few peaks, which makes interpretation problematic.

The main peak for combeite at about 34° 2$\theta$ (Fig. 2) appears as a single peak for glasses A and B and only appears as the typical split peak for higher concentrations of $CaF_2$. It was shown that mixed calcium sodium silicate glasses crystallise through the formation of solid solutions of several phases including combeite of different stoichiometry and a $Na_4CaSi_3O_9$ phase.[19] In sodium-rich glasses A and B we assume additional precipitation of $Na_4CaSi_3O_9$[20] which gives the principal XRD peak at about 34° 2$\theta$ overlapping with the split reflections of combeite. Absence of this phase on the XRD patterns of the compositions starting from C can be explained by the decrease in sodium content in the compositions.

$^{29}$Si MAS NMR spectra (Fig. 3a) for the heat-treated crystalline sample E show peaks in the range of $Q^3$ (−85 ppm) and $Q^4$ (−90 ppm). However, $Q^2$ in ring structures gives similar chemical shifts to $Q^4$.[20] As the six-membered ring combeite[21] is the main crystal phase, the peak at −90 ppm corresponds to one of the sites in the silica ring.[20,22] The peak at −85 ppm can then be explained by the remaining glass phase, which after crystallisation of combeite has a higher NC and therefore mostly a $Q^3$ structure. The fact that combeite is the main crystal structure in glasses A to E also suggests that in the amorphous glasses silica ring structures might also be present. This can explain the position of the $Q^3$ shoulder (−92 ppm) which is more negative than usually assigned to $Q^3$ units.

The presence of cuspidine detected by XRD is consistent with the change in $^{29}$Si NMR peak position (−82 ppm) towards $Q^1$ structure for crystallised sample F (Fig. 3a). Cuspidine has not been obtained as a single crystalline phase in our glasses unlike in low sodium glasses of Hayashi *et al.*[23] This is primarily because of a lower NC of 1.6 for the glasses designed by Hayashi *et al.* compared to our compositions.

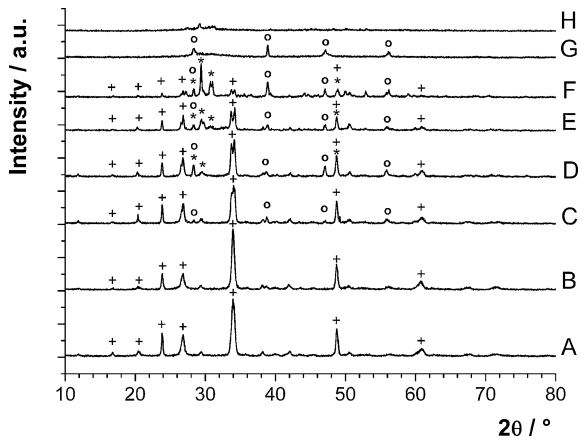


**Fig. 2** XRD patterns of heat-treated crystalline samples A to H (from bottom to top). Crystal phases are combeite (+), cuspidine (*) and calcium fluoride (○).

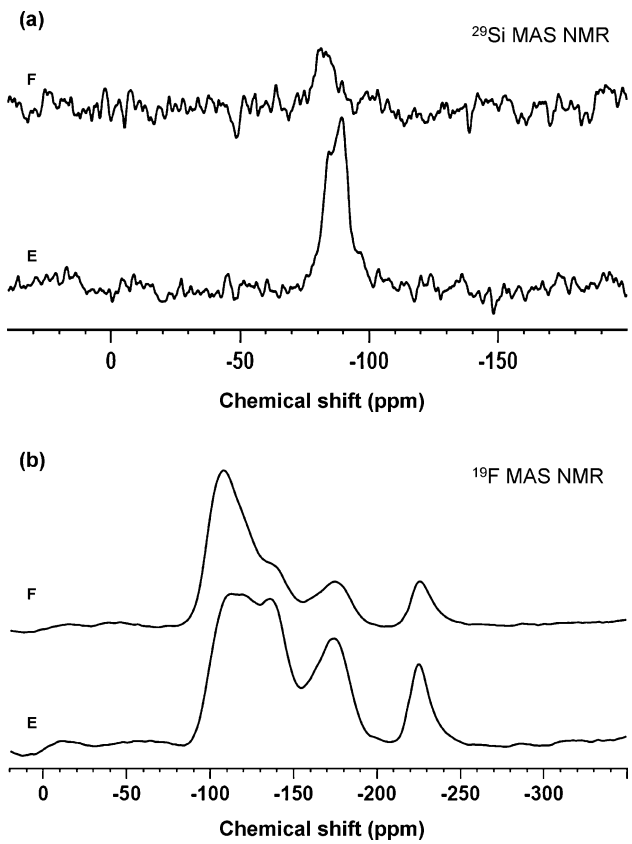


**Fig. 3** (a) $^{29}$Si MAS NMR spectra of heat-treated crystalline samples E (bottom) and F (top) and (b) $^{19}$F MAS NMR spectra of heat-treated crystalline samples E (bottom) and F (top).

### Structural role of fluoride and sodium ions

In the $^{19}F$ MAS NMR spectrum (Fig. 4) of the sodium-free glass (H) a single peak at −89 ppm corresponds to F–Ca(*n*) species as observed previously in calcium fluorosilicate glasses.[16,17] This peak is at higher chemical shifts than F–Ca(4) or F–Ca(3) in crystalline species due to slightly longer Ca–F distances in amorphous glasses.[24] In glasses B to G the peak at about −220 ppm is close to the position of the hexa-coordinated F–Na(6) species[25] and, thus, corresponds to complexes with sodium.

The signals between −115 and −165 ppm (Fig. 4) can be assigned to mixed sodium calcium fluoride species.[26,27] Hayashi *et al.*[26] report their chemical shifts relative to hexafluorobenzene ($C_6F_6$), and conversion to the scale relative to trichlorofluoromethane ($CFCl_3$) using a −164.9 ppm chemical shift value for $C_6F_6$ is found in Table 2. Their spectra show three broad peaks, which the authors assign to (a) F–Ca(4), F–Ca(3)Na(1) and F–Ca(2)Na(2) species in tetrahedral coordination, (b) F–Ca(1)Na(4) in pentahedral coordination and (c) F–Na(6) in hexahedral coordination.

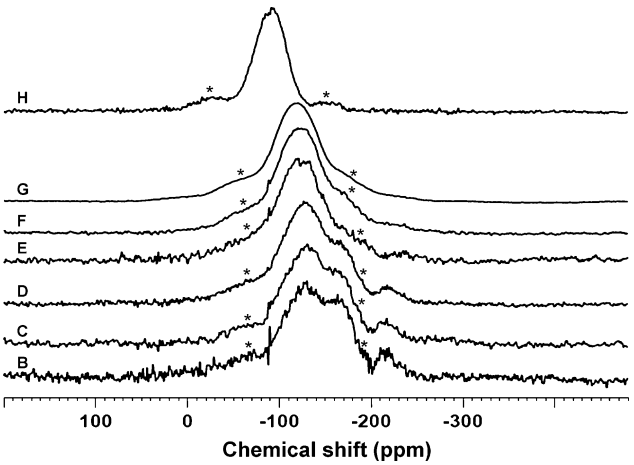


**Fig. 4** $^{19}F$ MAS NMR spectra of glasses B (bottom) to H (top). Spinning side bands are marked by an asterisk.

**Table 2** $^{19}F$ MAS NMR chemical shift references found in literature[25,26]

| Species | $^{19}F$ Chemical shift in ppm | |
|---|---|---|
| | Relative to $C_6H_6$ | Relative to $CFCl_3$ |
| F–Ca(4), F–Ca(3)Na(1), F–Ca(2)Na(2), (tetrahedral coordination) | 60.5 | −104.4 |
| | 58.3 | −106.6 |
| | 50.6 | −114.3 |
| | 38.1 | −126.8 |
| | 32.0 | −132.9 |
| | 26.4 | −138.5 |
| F–Ca(1)Na(4) (pentahedral coordination) | −8.2 | −173.1 |
| | −9.9 | −174.8 |
| | −10.4 | −175.3 |
| | −10.9 | −175.8 |
| F–Na(6) (hexahedral coordination) | −56.6 | −221.5 |
| | −59.4 | −224.3 |
| | −62.0 | −226.9 |
| Si–F–Ca(*n*) | — | −123 |
| | | −129 |
| | | −135 |
| Si–F–Na(2) | — | −152 |

For glasses B to D we clearly see three main peaks at about −130, −165 and −220 ppm (Fig. 4). We assign the peak at −165 ppm to F–Ca(2)Na(2), whereas the observed signals at −130 ppm in glasses B to D and −115 ppm in E to G are attributed to overlapping/unresolved signals from F–Ca(4) (at −108 ppm) and F–Ca(3)Na(1) (at −138 ppm). The presence of 5- or 6-coordinated fluorine in mixed calcium–sodium environment in this region should also be considered. Due to the high calcium concentration in glasses E to G the dominating contribution from F–Ca(4) causes the shift of the total signal towards the site of F–Ca(4).

$^{19}F$ MAS NMR spectra of the heat-treated samples (Fig. 3b) demonstrate a significant increase in structural order of the fluoride sites compared to the untreated glasses. This is consistent with the fluorine-containing phases identified on XRD patterns (fluorite and cuspidine). In addition to peaks at about −175 and −225 ppm, the spectra of heat-treated crystalline samples E and F clearly illustrate that the broad peak between about −115 and −130 ppm actually consists of at least two individual peaks at about −108 and −138 ppm. The signal from cuspidine is not clearly resolved on the $^{19}F$ NMR spectra due to severe overlaps in the region from −100 to −110 ppm. We assign the peak at −175 ppm in the crystalline samples to a mixed sodium calcium coordination which is an intermediate to the pure sodium site F–Na(6) at −225 ppm. Hayashi *et al.*[26] assigned this to a pentahedral coordination of fluorine in F–Ca(1)Na(4), however, we do not exclude the possibility that it could be hexahedral F–Na(4)Ca(2) species.

For higher fluorine concentrations, the relative intensities of the $^{19}F$ NMR peaks in the region from −165 to −225 ppm in glasses and their crystalline counterparts decrease and only shoulders are visible for some of these resonances. This is caused by the fact that with increasing amounts of $CaF_2$ the concentration of sodium decreases and thus fluorine preferentially complexes calcium, rather than sodium.

The $^{19}F$ NMR data presented above provide further evidence for the absence of NBF and Si–F–Ca(*n*) and Si–F–Na(*n*) species, the signals of which would be expected in the range between −123 and −152 ppm (Table 2).[25] This is in agreement with the findings by Hayashi *et al.* who investigated the effect of fluorine addition on the network connectivity of glasses in the system $SiO_2$–CaO–$CaF_2$ using X-ray photoelectron spectroscopy (XPS).[18] According to their results fluorine does not affect the network connectivity or the concentration of NBO, but is coordinated with $Ca^{2+}$. This was further confirmed by $^{19}F$ NMR investigations by Watanabe *et al.*[28] In glasses with a network connectivity around 2, the presence of Si–F bonds is unlikely since there is a large concentration of NBO in the glasses and $Si^{4+}$ has a higher affinity for $O^{2-}$ ions than for $F^-$ ions.[16] Thus this strongly suggests that fluorine complexes only calcium and sodium.

Transition temperature ($T_g$) of the glasses decreased with increasing $CaF_2$ content (Fig. 5) which further indicates that fluorine was not lost in significant amounts. Crystallisation onset ($T_{c,ons}$) and peak ($T_{c,peak}$) temperatures also decreased with increasing $CaF_2$ content. The decrease in $T_g$ can also be explained by the fact that fluorine is complexing calcium: in

 

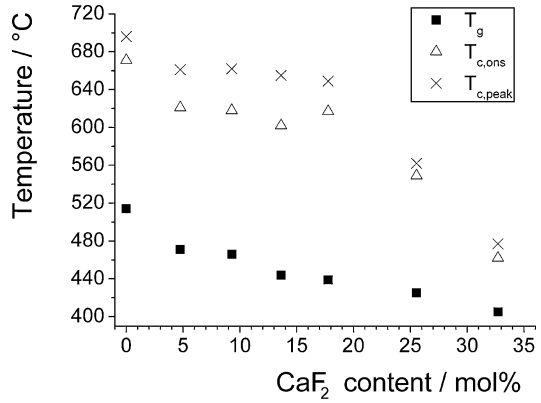


**Fig. 5** Glass transition temperature ($T_g$), crystallisation onset ($T_{c,ons}$) and crystallisation peak ($T_{c,peak}$) temperatures *vs.* $CaF_2$ content. The error is less than the size of the points.

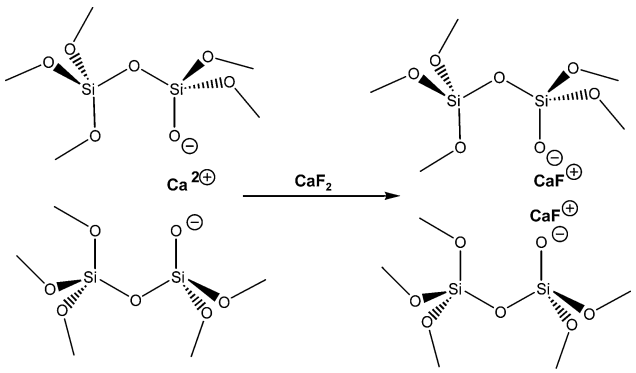


**Fig. 6** Illustration of the hypothetical effect of $CaF_2$ addition on silicate network.

fluorine-free glass A, divalent calcium ions bind together silicate anions by electrostatic forces and the calcium ions effectively act as ionic bridges between two NBO. When $CaF_2$ is added (Fig. 6), hypothetical $CaF^+$ species are added to the silicate ions which reduce the electrostatic forces between non-bridging oxygens considerably and results in a decrease in $T_g$.[18,29,30]

$^{23}$Na MAS NMR spectra of glasses A, C and E to G (Fig. 7) exhibit a single broad peak centred between −1 and −5 ppm. Despite the broadness of the peaks there do appear to be sites within the glass between 4 and 7 ppm, with a sharp feature at 4 ppm which is particularly pronounced in sample A. In glass ceramics, the $^{23}$Na MAS NMR signal from NaF varies between 5 and 7 ppm depending on the crystal size.[31] Therefore, the appearance of a small shoulder at *ca.* 7 ppm can be explained by complexing sodium with fluorine with increasing fluorine concentrations. After crystallisation (Fig. 8), a very sharp peak appears at 7 ppm due to an increase in structural order of the fluorine environment as seen in $^{19}$F MAS NMR.

Gradual replacement of combeite by the fluorine-containing phases cuspidine and fluorite, which was seen in the XRD results, should be expected to be associated with the evolution of the $^{23}$Na NMR signal of the crystallised samples (Fig. 8) at 13 and −1 ppm along the series. Unfortunately, there are no $^{23}$Na NMR reference spectra for combeite crystals of any stoichiometry. Moreover, the precipitation of a $2Na_2SiO_3$–$CaSiO_3$ or

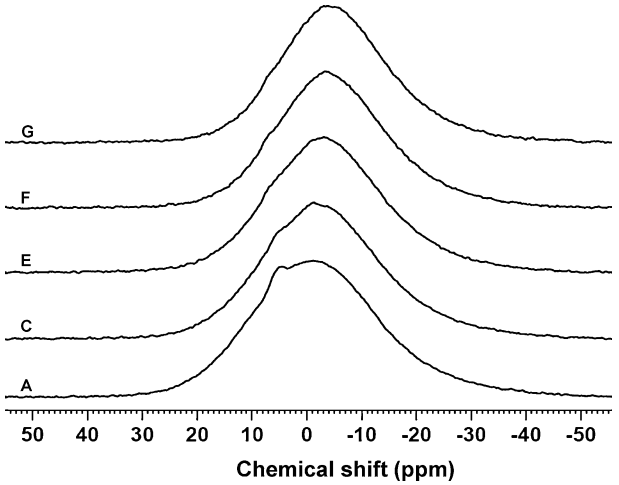


**Fig. 7** $^{23}$Na MAS NMR spectra of glasses A, C and E to G.

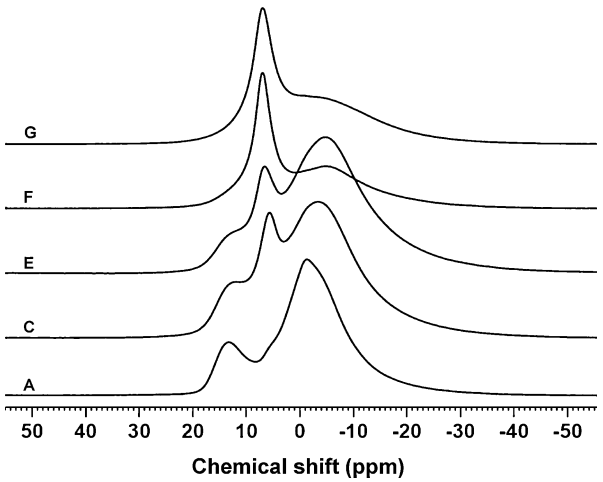


**Fig. 8** $^{23}$Na MAS NMR spectra of crystalline samples A, C and E to G.

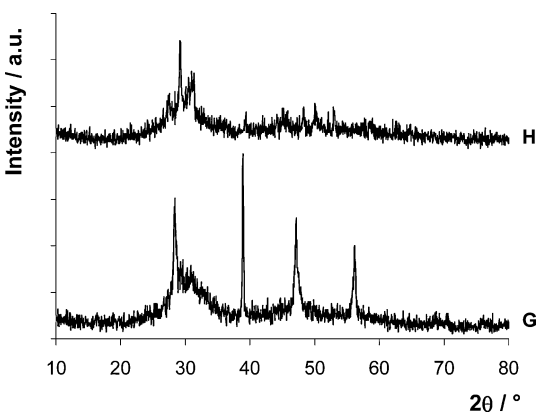


**Fig. 9** XRD patterns of heat-treated crystalline samples G (bottom) and H (top) showing crystalline diffraction pattern superimposed on an amorphous halo.

$Na_4CaSi_3O_9$ phase in sodium-rich compositions of the series (as seen from the XRD data) additionally complicates interpretation of the $^{23}$Na NMR spectra for the crystalline samples. The broad

peak at −1 ppm for crystallised sample G (Fig. 8) is likely to be caused by the significant amount of glassy phase found by XRD (Fig. 9).

$^{23}$Na 3QMAS NMR spectra for samples A and G are given in Fig. 10 and 11 and confirm the presence of multiple sodium sites in the glasses. The distinctive shoulder in the fluorine-free glass (A) appearing on the MAS spectrum (Fig. 7) at 4 ppm has an isotropic chemical shift at *ca.* 8 ppm overlapping to a broad featureless signal as seen in Fig. 10. This result agrees with the simulation of the $^{23}$Na 3QMAS NMR experimental spectrum for Bioglass® 45S5 containing at least three different sites[32] with one of them giving a distinctively narrow resonance. The origin of this narrow signal is not clear and could also arise from surface hydration. Comparison of these deconvolution results with an NMR study on bioactive glasses by Lockyer *et al.*[33] indicates that the broad site perhaps dominates in the low field spectra, giving a nearly −10 ppm value for MAS shift at 8.45 T. In the glass with the highest fluorine content (glass G) the signal becomes broader, but does show at least two lines one of which has a larger quadrupolar constant (site I), as shown in Fig. 11, but as in glass A no sharp features are detected. A slight shift to more negative values of the broad $^{23}$Na resonance indicates an increase in the mean coordination number of sodium in the glasses[34] moving from A to G, probably arising from a decrease in sodium content within the series. This is consistent with the observations by Lusvardi *et al.*[14]

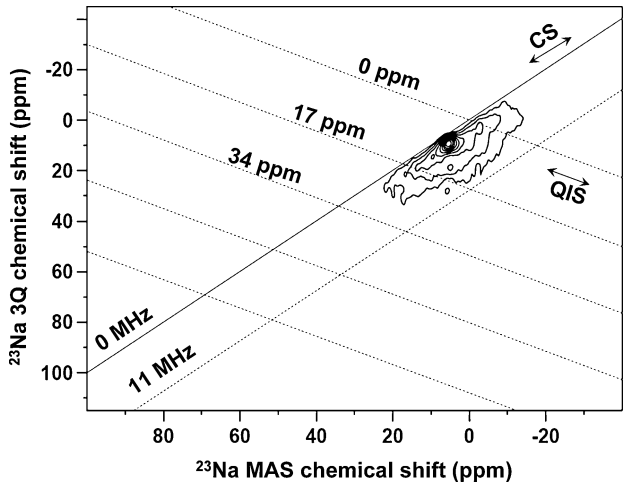


**Fig. 10** $^{23}$Na 3QMAS NMR spectrum of glass A. The lines inside the spectrum illustrate the position of the isotropic chemical shift and quadrupolar product. The distribution of isotropic chemical shift (CS) and quadrupolar isotropic shift is indicated by arrows. 10 contours are drawn every 10% from 10 to 100% of spectral intensity.

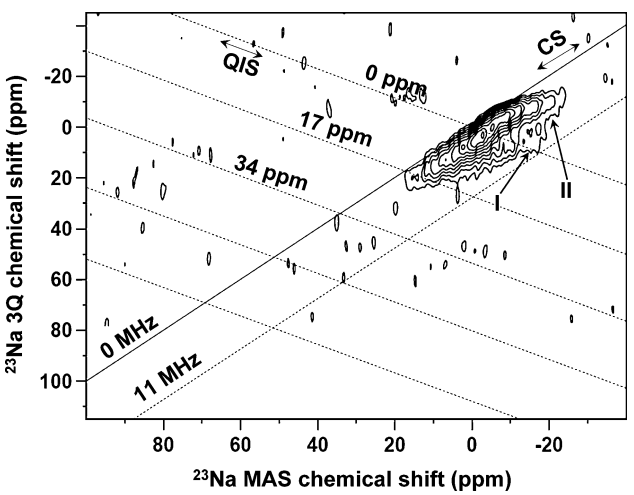


**Fig. 11** $^{23}$Na 3QMAS NMR spectrum of glass G. The lines inside the spectrum illustrate the position of the isotropic chemical shift and quadrupolar product. The distribution of isotropic chemical shift (CS) and quadrupolar isotropic shift is indicated by arrows. 10 contours are drawn every 10% from 10 to 100% of spectral intensity. Features of at least two different sites are distinguished: site I has a larger quadrupolar constant than site II.

### Structural role of phosphate

$^{31}$P MAS NMR spectra (Fig. 12) show a single peak corresponding to orthophosphate, $Q^0$, which shows that phosphate is not part of the actual glass network backbone and no Si–O–P bonds are present. These findings are in contrast to the modelling results by Lusvardi *et al.* who found that increasing amounts of fluoride ions forces phosphate groups to bond to silicon atoms by removing the modifier ions Ca and Na from the silicate glass network.[14] Orthophosphate groups are charge balanced by cations, which in our glasses are $Na^+$, $Ca^{2+}$ and the hypothetical $CaF^+$ species. While we introduce $CaF_2$ into the glass, the chemical shift of the orthophosphate peak moves from 9 ppm (glass A) to 6 ppm (glass G) and 3 ppm (sodium-free glass H). This agrees with the findings by Lockyer *et al.* and Elgayar *et al.* who substituted CaO for $Na_2O$ in bioactive glass compositions and observed a shift to less positive peak positions (towards 0 ppm) with increased amounts of CaO.[10,33] Lockyer *et al.* explained this by differences in the electronegativities of $Na^+$ and $Ca^{2+}$, which result in displacement of charge from the oxygen and hence from the P–O bond. This increases the electronic shielding of the phosphorus and produces a more negative chemical shift. Alternatively, the higher field of the $Ca^{2+}$ cation drives the $^{31}$P chemical shift towards more negative values compared to the effect of the lower potential of $Na^+$.[35] In our system, however, we

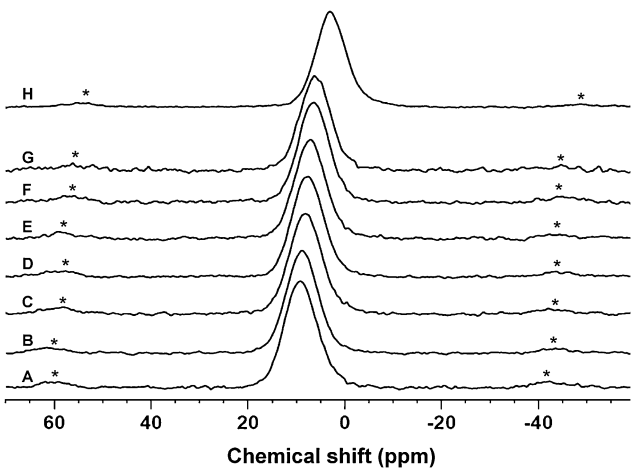


**Fig. 12** $^{31}$P MAS NMR spectra of glasses A (bottom) to H (top). Spinning side bands are marked by an asterisk.

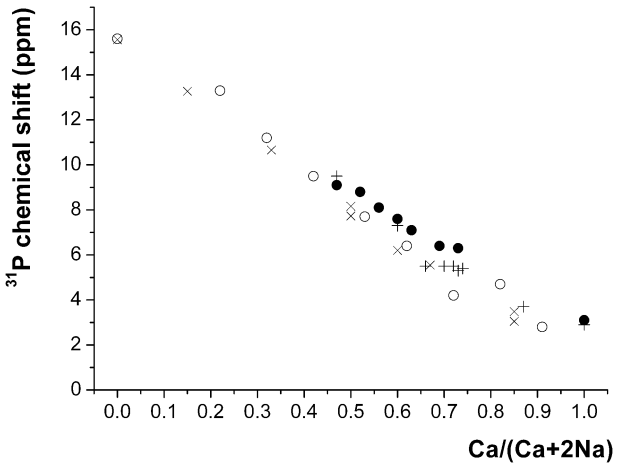


**Fig. 13** $^{31}$P MAS NMR chemical shift *vs.* calcium content as a fraction of total calcium and sodium (all in at%): ● our results, + Elgayar *et al.*,[10] ○ Lockyer *et al.*[33] and × Grussaute *et al.*[36]

have an additional species potentially contributing to the chemical shift of orthophosphate, the hypothetical $CaF^+$ unit. We therefore compared our $^{31}$P MAS NMR results with those in the literature.[10,33,36] Fig. 13 illustrates the $^{31}$P isotropic chemical shift trend graphically: it shows the $^{31}$P NMR chemical shift *vs.* calcium as a fraction of total calcium and sodium (each expressed in at%) and our results show very good agreement with those found in the literature. Thus, the hypothetical $CaF^+$ species do not seem to contribute to the charge balancing of the orthophosphate species and the evolution of the $^{31}$P chemical shift is governed by the reduction of the sodium proportion in glasses A to G. Additionally, the results in Fig. 13 reveal the disordered character of the phosphate environment, *i.e.* the cations charge balancing the orthophosphate units while $CaF_2$ is introduced in glass. This indicates that there is no preferential association with either sodium or calcium ions, and these will therefore be present in a ratio consistent with that of the overall glass composition.[33] This differs from the conclusions of Lusvardi *et al.* who suggested an ultimate preference of the phosphate units for calcium cations.[14] We would expect formation of mixed sodium calcium orthophosphates during crystallisation in our glasses, although the amount of this phase is perhaps too low for detection by XRD.

### Impact on bioactivity

The knowledge of the structure of fluoride-containing bioactive glasses can be applied to previous studies of bioactive glasses in the literature: Table 3 shows four compositions taken from Fujii *et al.*[37] Using the fact that fluorine complexes Ca and Na, we have calculated the theoretical and experimental NC which determines the proportions of the $Q^n$ species present and can also be used to predict the bioactivity. There is an excellent agreement between our predicted NC and their experimental determined values (Table 3). Furthermore taking the value of an NC = 2.4 as the cut off for bioactivity,[9] the bioactivity of the glasses can be successfully predicted: the glass (F10C40S50) with a theoretical NC of 2.4 gave an experimental NC of 2.60. *In vitro* formation of apatite in simulated body fluid is often taken as an indicator of bioactivity,[38] and the glass F10C40S50 showed no formation of apatite within one week while all other compositions with NC below 2.4 did.

**Table 3** Synthetic glass composition in mol%, theoretical (NC calculated assuming fluorine complexes calcium) and experimental network connectivity of species and experimental bioactivity (in terms of formation of an apatite layer in simulated body fluid within 3 days) of glasses by Fujii *et al*[37]

| Glass | $SiO_2$ | CaO | NaF | Theor. NC | Exp. NC (NMR) | Bioactive |
|---|---|---|---|---|---|---|
| C50S50 | 50 | 50 | 0 | 2.0 | 2.11 | Yes |
| F10C40S50 | 50 | 40 | 10 | 2.4 | 2.60 | No |
| F10C45S45 | 45 | 45 | 10 | 2.0 | 2.05 | Yes |
| F10C50S40 | 40 | 50 | 10 | 1.5 | 1.63 | Yes |

This shows that (a) NC calculations can be used to successfully predict the bioactivity of glasses and (b) knowledge of the glass structure is very important when designing new bioactive glasses.

## Conclusions

To the best of our knowledge, this is the first multi-nuclei characterisation of the structure of fluoride-containing bioactive glasses. Our detailed structural investigations result in a thorough understanding of the structure–property relationship in this class of bioactive glasses. We have demonstrated that in fluoride-containing bioactive glasses formation of Si–F bonds or non-bridging fluorines does not occur to a significant extent. Instead, fluorine complexes calcium and sodium and is present principally as mixed calcium sodium fluoride species. This means that if calcium fluoride is substituted for network modifiers such as CaO or $Na_2O$, it results in crosslinking of the network, an increase in network connectivity and thus reduced reactivity and bioactivity of the glass. By assuming that fluorine complexes calcium and keeping the ratio of network former to network modifier constant when adding calcium fluoride, network connectivity and subsequently bioactivity are kept constant. The results of this study will be valuable in designing and producing new fluoride-containing bioactive glasses for use as reconstructive material for bone and other hard tissue, but they are also of interest for the design of other fluoride-containing silica glass systems with a high concentration of non-bridging oxygens, *e.g.* mould flux systems.

## References

1 J. D. B. Featherstone, *J. Am. Dental Assoc., JADA*, 2000, **131**, 887–899.
2 T. T. Thuy, H. Nakagaki, K. Kato, P. A. Hung, J. Inukai, S. Tsuboi, H. Nakagaki, M. N. Hirose, S. Igarashi and C. Robinson, *Arch. Oral. Biol.*, 2008, **53**, 1017–1022.
3 P. Vestergaard, N. R. Jorgensen, P. Schwarz and L. Mosekilde, *Osteoporosis Int.*, 2008, **19**, 257–268.
4 J. Aaseth, M. Shimshi, J. L. Gabrilove and G. S. Birketvedt, *J. Trace Elem. Exp. Med.*, 2004, **17**, 83–92.
5 W. Vogel and W. Höland, *Angew. Chem., Int. Ed. Engl.*, 1987, **26**, 527–544.
6 L. L. Hench, D. B. Spilman, J. W. Hench, University of Florida, *Fluoride-modified bioactive glass (Bioglass) and its use as implant material*, *US Pat.*, 4 775 646, 1988.
7 L. L. Hench, *J. Mater. Sci. Mater. Med.*, 2006, **17**, 967–978.

8 B. J. Tai, Z. Bian, H. Jiang, D. C. Greenspan, J. Zhong, A. E. Clark and M. Q. Du, *J. Clin. Periodontol.*, 2006, **33**, 86–91.
9 R. Hill, *J. Mater. Sci. Lett.*, 1996, **15**, 1122–1125.
10 I. Elgayar, A. E. Aliev, A. R. Boccaccini and R. G. Hill, *J. Non-Cryst. Solids*, 2005, **351**, 173–183.
11 D. G. Cory and W. M. Ritchey, *J. Magn. Reson.*, 1988, **80**, 128–132.
12 J. P. Amoureux and C. Fernandez, *Solid State Nucl. Magn. Reson.*, 1998, **10**, 211–223.
13 D. Massiot, F. Fayon, M. Capron, I. King, S. Le Calve, B. Alonso, J. O. Durand, B. Bujoli, Z. H. Gan and G. Hoatson, *Magn. Reson. Chem.*, 2002, **40**, 70–76.
14 G. Lusvardi, G. Malavasi, M. Cortada, L. Menabue, M. C. Menziani, A. Pedone and U. Segre, *J. Phys. Chem. B*, 2008, **112**, 12730–12739.
15 R. Hill, D. Wood and M. Thomas, *J. Mater. Sci.*, 1999, **34**, 1767–1774.
16 R. G. Hill, N. Da Costa and R. V. Law, *J. Non-Cryst. Solids*, 2005, **351**, 69–74.
17 Q. Zeng and J. F. Stebbins, *Am. Mineral.*, 2000, **85**, 863–867.
18 M. Hayashi, N. Nabeshima, H. Fukuyama and K. Nagata, *ISIJ Int.*, 2002, **42**, 352–358.
19 V. M. Fokin and E. D. Zanotto, *J. Non-Cryst. Solids*, 2007, **353**, 2459–2468.
20 J. Schneider, V. R. Mastelaro, H. Panepucci and E. D. Zanotto, *J. Non-Cryst. Solids*, 2000, **273**, 8–18.
21 H. Ohsato, Y. Takeuchi and I. Maki, *Acta Crystallogr., Sect. C: Cryst. Struct. Commun.*, 1986, **42**, 934–937.
22 M. D. O'Donnell, S. J. Watts, R. V. Law and R. G. Hill, *J. Non-Cryst. Solids*, 2008, **354**, 3554–3560.
23 M. Hayashi, T. Watanabe, K. Nagata and S. Hayashi, *ISIJ Int.*, 2004, **44**, 1527–1533.
24 N. Boden, P. K. Kahol, A. Mee, M. Mortimer and G. N. Peterson, *J. Magn. Reson.*, 1983, **54**, 419–426.
25 T. J. Kiczenski and J. F. Stebbins, *J. Non-Cryst. Solids*, 2002, **306**, 160–168.
26 M. Hayashi, T. Watanabe, H. Nakada and K. Nagata, *ISIJ Int.*, 2006, **46**, 1805–1809.
27 J. F. Stebbins and Q. Zeng, *J. Non-Cryst. Solids*, 2000, **262**, 1–5.
28 T. Watanabe, M. Hayashi, S. Hayashi, H. Fukuyama, K. Nagata. *Solid-state F-19 NMR on CaO–$SiO_2$–$CaF_2$ glasses*. Johannesburg, The South African Institute of Mining and Metallurgy, 2004, pp. 699–706.
29 T. Bååk and A. Ölander, *Acta Chem. Scand.*, 1955, **9**, 1350–1354.
30 P. M. Bills, *J. Iron Steel Inst.*, 1963, **201**, 133–140.
31 J. W. Zwanziger, U. Werner-Zwanziger, E. D. Zanotto, E. Rotari, L. N. Glebova, L. B. Glebov and J. F. Schneider, *J. Appl. Phys.*, 2006, **99**, DOI: 10.1063/1.2191731.
32 A. Angelopoulou, V. Montouillout, D. Massiot and G. Kordas, *J. Non-Cryst. Solids*, 2008, **354**, 333–340.
33 M. W. G. Lockyer, D. Holland and R. Dupree, *J. Non-Cryst. Solids*, 1995, **188**, 207–219.
34 X. Y. Xue and J. F. Stebbins, *Phys. Chem. Miner.*, 1993, **20**, 297–307.
35 R. J. Kirkpatrick and R. K. Brow, *Solid State Nucl. Magn Reson.*, 1995, **5**, 9–21.
36 H. Grussaute, L. Montagne, G. Palavit and J. L. Bernard, *J. Non-Cryst. Solids*, 2000, **263**, 312–317.
37 E. Fujii, K. Kawabata, H. Yoshimatsu, S. Hayakawa, K. Tsuru and A. Osaka, *J. Ceram. Soc. Jpn.*, 2003, **111**, 762–766.
38 T. Kokubo and H. Takadama, *Biomaterials*, 2006, **27**, 2907–2915.

 